Astronomical Journal MS #340334 Version 2
Preprint typeset using LaTeX style emulateapj v. 2/16/10

DISCOVERY OF A NOVA-LIKE CATACLYSMIC VARIABLE IN THE KEPLER MISSION FIELD

Kurtis A. Williams
Department of Astronomy, University of Texas, 1 University Station C1400, Austin, TX 78712, USA

Domitilla de Martino
INAF–Osservatorio di Capodimonte, Moiarello 16, 80131, Napoli, Italy

Roberto Silvotti
INAF–Osservatorio Astronomico di Torino, strada dell'Osservatorio 20, 10025 Pino Torinese, Italy

Ivan Bruni
INAF–Osservatorio Astronomico di Bologna, via Ranzani 1, 40127 Bologna, Italy

Patrick Dufour
Département de physique, Université de Montréal
Montréal, QC H3C 3J7, Canada

Thomas S. Riecken, Martin Kronberg, Anjum Mukadam
Astronomy Department, Box 351580, University of Washington, Seattle, WA 98115, USA

and

G. Handler
Institut für Astronomie, Universität Wien, Türkenschanzstrasse 17, A-1180 Wien, Austria

Astronomical Journal MS #340334 Version 2

ABSTRACT

We announce the identification of a new cataclysmic variable star in the field of the Kepler Mission, KIC J192410.81+445934.9. This system was identified during a search for compact pulsators in the Kepler field. High-speed photometry reveals coherent large-amplitude variability with a period of 2.94 h. Rapid, large-amplitude quasi-periodic variations are also detected on time scales of ≈ 1200 s and ≈ 650 s. Time-resolved spectroscopy covering one half photometric period shows shallow, broad Balmer and He I absorption lines with bright emission cores as well as strong He II and Bowen blend emission. Radial velocity variations are also observed in the Balmer and He I emission lines that are consistent with the photometric period. We therefore conclude that KIC J192410.81+445934.9 is a nova-like variable of the UX UMa class in or near the period gap, and it may belong to the rapidly growing subclass of SW Sex systems. Based on 2MASS photometry and companion star models, we place a lower limit on the distance to the system of ~ 500 pc. Due to limitations of our discovery data, additional observations including spectroscopy and polarimetry are needed to confirm the nature of this object. Such data will help to further understanding of the behavior of nova-like variables in the critical period range of $3 - 4$ h, where standard cataclysmic variable evolutionary theory finds major problems. The presence of this system in the Kepler mission field-of-view also presents a unique opportunity to obtain a continuous photometric data stream of unparalleled length and precision on a cataclysmic variable system.

Subject headings: binaries: close — novae, cataclysmic variables

1. INTRODUCTION

Cataclysmic variables (CVs) are close binary systems in which a white dwarf (WD) accretes material from a companion star. The secondary star is a late-type dwarf filling its Roche lobe, and, in most cases, the overflowing material forms an accretion disk around the WD primary.

One class of CVs is the nova-like (NL) system. Historically, a NL system not showing magnetic characteristics is classified as a UX UMa star (Dhillon 1996). Non-magnetic NLs exhibit the same variety of optical spectra as the dwarf novae in outburst, ranging from pure emission-line spectra (high inclination) to pure absorption-line spectra (low inclination). Therefore, NLs are characterized by relatively high mass accretion rates.

The classification scheme may improve with consideration of more precise photometric and spectroscopic characteristics. Systems in the 3–4 h orbital period range can be identified as VY Scl stars when they are found to undergo low states or can be identified as SW Sex stars when their spectra display single-peaked emission features irrespective of inclination angle with absorption components variable along the orbital period

kurtis@astro.as.utexas.edu

Table 1
Astrometric and Photometric Properties of KIC J1924+4459

Parameter	Value	Date	Source
RA(J2000)	$19^{\rm h}24^{\rm m}10\overset{\rm s}{.}82$	···	KIC10[a]
Dec(J2000)	$+44°59'34\overset{''}{.}9$	···	KIC10[a]
$\mu_{\rm RA}$	24 ± 8 mas yr^{-1}	1980.90	USNO-B1.0
$\mu_{\rm Dec}$	34 ± 17 mas yr^{-1}	1980.90	USNO-B1.0
B_p	15.22	1951.5195	USNO-B1.0
R_p	···	1951.5195	USNO-B1.0
B_p	15.59	1976.56	YB6[b]
V_p	15.79	1976.56	YB6[b]
B_p	15.30	1988.4695	USNO-B1.0
R_p	15.36	1991.5795	USNO-B1.0
I_p	15.72	1990.4463	USNO-B1.0
J	16.839 ± 0.137	1998.436	2MASS
H	≥ 16.736	1998.436	2MASS
K	≥ 16.536	1998.436	2MASS
g	16.182	2007.1[c]	KIC10[a]
$g-r$	−0.116	2007.1[c]	KIC10[a]
$r-i$	−0.091	2007.1[c]	KIC10[a]
$r-z$	−0.214	2007.1[c]	KIC10[a]

[a] Kepler Input Catalog v. 10, Latham 2008
[b] USNO Yellow-Blue Catalog v. 6, D. Monet (private communications)
[c] KIC10 photometry is a weighted average of data obtained 2006.281, 2007.412, and 2007.486

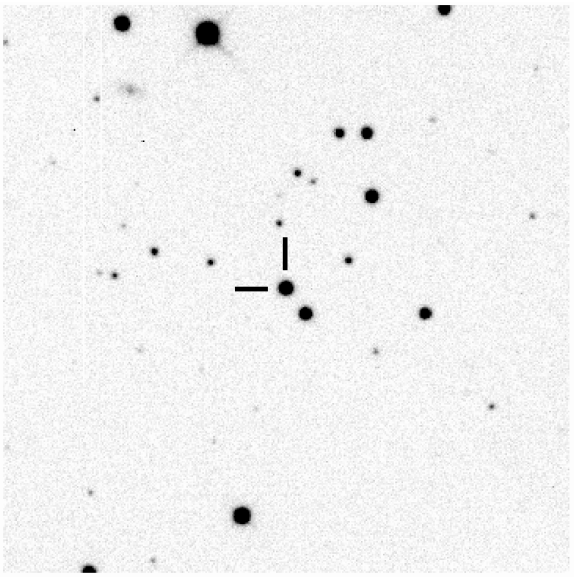

Figure 1. Finder chart for KIC J1924+4459. The chart is 2′ on a side; north is up, east to the left. The system is centered and marked with tick marks. This image was obtained at McDonald Observatory through a BG40 filter.

(Thorstensen et al. 1991; Warner 1995; Dhillon 1996). Recently, the SW Sex class has been claimed to be the dominant population of the 3–4 h orbital period CV systems (e.g., Rodríguez-Gil et al. 2007a,b). NLs, generally not (yet) known to display the above characteristics are classified as UX UMa stars from the presence of strong absorption features in Balmer lines with superposed narrow emission cores as well as emission lines of He I and He II. The detection of emission in these lines are clear signs of accretion and therefore cannot be mistaken with non-accreting WD+M binaries.

Although the historical definition of NL systems is of a non-magnetic CV, there is considerable evidence that magnetism is present in at least some NLs, and that magnetism may be the force behind many of the defining characteristics of SW Sex systems. Based on profiles of emission lines during eclipses, Williams (1989) proposed that magnetic accretion columns could be present in NLs. Magnetism was also invoked to explain the complex behavior in the SW Sex star V795 Her (e.g., Thorstensen 1986; Casares et al. 1996) and confirmed with the detection of variable circular polarization in the system (Rodríguez-Gil et al. 2002). Variable circular polarization has also been detected in the SW Sex stars LS Peg (Rodríguez-Gil et al. 2001) and RX J1643.7+3402 (Rodríguez-Gil et al. 2009). Other evidence of magnetism has also been observed in multiple SW Sex systems, including emission line flaring in systems such as BT Mon (Smith et al. 1998) and V533 Her (Rodríguez-Gil & Martínez-Pais 2002) and far UV / X-ray signatures of magnetism in objects like DW UMa (Hoard et al. 2003) and LS Peg (Baskill et al. 2005). Clearly magnetism plays an important role in many, if not all, SW Sex stars.

We report on the discovery of a NL, UX UMa-type system, KIC J192410.81+445934.9 (Kepler ID 8751494, hereafter KIC J1924+4459), in the field-of-view of the Kepler Mission. This discovery was made as part of an as-yet unsuccessful search for compact pulsators (WDs and subdwarf B stars) in the Kepler Input Catalog. Time-series photometric observations of compact pulsator candidates were obtained at the TNG, McDonald Observatory, and the BOAO Observatory (Seung Lee-Kim, private communication) without any clear detection of pulsations in any of the observed targets. Some preliminary TNG results are presented by Silvotti et al. (2009).

The detection of a photometric periodicity at 2.94 h in KIC J1924+4459, potentially also detected in the radial velocities of the emission lines, and the detection of rapid non-periodic variability hints that this star may belong to the growing class of SW Sex systems.

2. PHOTOMETRIC OBSERVATIONS AND ANALYSIS

2.1. *Selection and Time-Series Photometry*

Potential pulsating white dwarfs were selected via their location in the reduced proper motion diagram based on photometric and astrometric data in the Kepler Input Catalog (Latham 2008). In particular, KIC J1924+4459 was flagged as a potential ZZ Ceti pulsator; its astrometric and photometric properties from the Kepler Input Catalog are given in Table 1; a finder chart is given in Figure 1.

Initial time-series observations were obtained 24 August 2008 on the 3.6-m TNG telescope with the DOLORES imaging spectrograph. The imaging data were taken with the g-band filter with exposure times of 8 s; a short 0.98 h run revealed flux variations of $\gtrsim 10\%$. Photometric data were reduced using standard procedures in IRAF[1], including bias, flat-fielding, and sky subtraction. Aperture photometry was obtained for the target and

[1] IRAF is distributed by the National Optical Astronomy Observatories, which are operated by the Association of Universities for Research in Astronomy, Inc., under cooperative agreement with the National Science Foundation

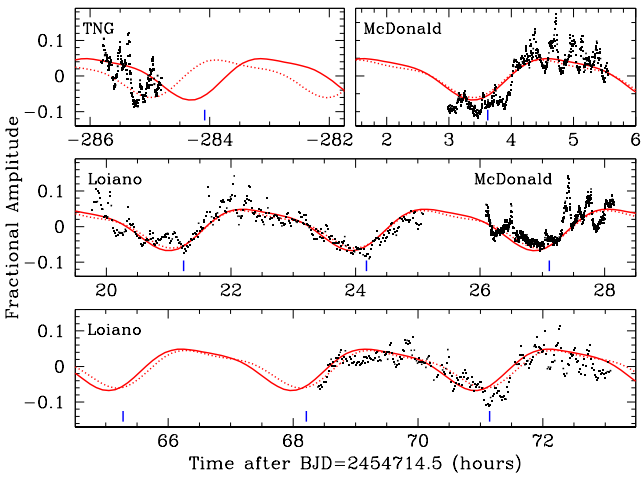

Figure 2. Time series photometry for KIC J1924+4459 from UT 24 August 2008 through UT 7 September 2008. Labels indicate the source of the data; the heavy curve is the best-fitting sinusoid plus first harmonic (see Section 2.2) from all data; the dotted curve is the best-fitting sinusoid plus first harmonic from the Loiano data alone. Time is given in hours relative to BJD 2454714.5; the horizontal scale in each panel is the same. Vertical tick marks indicate the predicted times of potential grazing eclipses in the Loiano data based on a potential grazing eclipse at $t = 24.175$ h.

several comparison stars. The flux ratios were obtained by dividing the counts of the target by the best combination (weighted mean) of three reference stars. These ratios were converted to fractional intensities by dividing the mean flux ratio. Barycentric corrections were also applied.

Additional time-series data were obtained at McDonald Observatory and the Bologna Astronomical Observatory. The McDonald observations were obtained with the Argos high-speed photometer on the 2.1-meter Struve Telescope; Argos uses a prime-focus, back-illuminated frame-transfer CCD to obtain uninterrupted time-series photometry (Nather & Mukadam 2004). Data were obtained through a BG40 filter with individual exposure times of 10 seconds; runs of 2.57 h and 2.06 h were obtained on UT 2008 September 5 and 6, respectively. Data were reduced in the manner described by Mullally et al. (2005) and Mullally et al. (2008) using the IRAF package *ccd_hsp* (O'Donoghue et al. 2000).

The Loiano/Bologna observations were obtained on UT 2008 September 5 and 7 at 1.5-meter Loiano telescope equipped with a BFOSC detector operated without a filter. Integration times were 40 s on September 5 and 45 s on September 7. A total of 332 and 269 frames were acquired during the 5.3 h and 4.7 h runs of the two nights, respectively. The data were reduced in the same manner as the TNG data.

The time-series data are shown in Figure 2.

2.2. *Photometric variability analysis*

2.2.1. *Short-term variability*

The light curves display large amplitude variations of 0.12 mag that appear to be periodic. The light curve shape is not sinusoidal, but shows sharp rises and structured decays. We then performed a Scargle analysis of the Loiano data that revealed a strong peak at 94.4 μHz and a secondary peak at 188 μHz. The latter peak is close to twice the frequency of the strong peak. We therefore fitted a composite sinusoidal function with a fundamental period of 2.9422 ± 0.0016 h (frequency $\nu = 8.1560 \pm 0.0051\,\mathrm{d}^{-1}$) and the first harmonic.

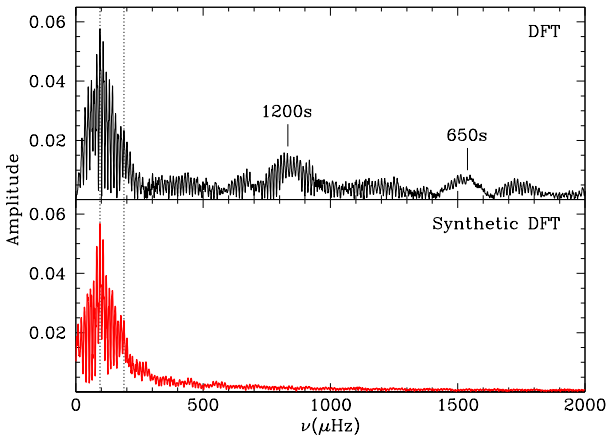

Figure 3. Discrete Fourier transforms of the combined McDonald and Loiano data sets (top) and of the synthetic light curve generated using the sinusoidal fits including the fundamental and first harmonic to the combined McDonald and Loiano photometry (bottom). Vertical lines indicate the frequencies of the fundamental and first harmonic. Also indicated in the DFT are two broad peaks of power likely related to the quasi-coherent variations observed in the light curves.

As the amplitudes of the variability were similar in both the unfiltered Loiano photometry and the BG40 McDonald photometry, and as the two data sets were interleaved, we combined the two data sets to more precisely constrain the periodicities in the data. Due to the large gap between the discovery photometry and our subsequent follow-up and the short duration of observation, we did not include the discovery TNG data in the combined analysis. A discrete Fourier transform (DFT) of the combined data (Fig. 3) shows a strong peak very near the frequency of the Loiano data peak. Again, we simultaneously fit a fundamental frequency and its first harmonic

$$f = A_0 \sin(2\pi \frac{t - t_{0,\mathrm{phot}}}{P_{\mathrm{phot}}}) + A_1 \sin(4\pi \frac{t - t_1}{P_{\mathrm{phot}}}), \qquad (1)$$

where f is the fractional amplitude. For the fundamental frequency, we derive a photometric period $P_{\mathrm{phot}} = 2.9358 \pm 0.0017$ h ($\nu = 8.1749 \pm 0.0070\,\mathrm{d}^{-1}$) with an amplitude $A_0 = 0.0556 \pm 0.0014$ and $t_{0,\mathrm{phot}}(\mathrm{BJD}) = 2454715.52547(74)$. For the first harmonic, $A_1 = 0.0133 \pm 0.0014$ and $t_1(\mathrm{BJD}) = 2454715.57688(148)$. Figure 2 shows this fit overplotted on the photometric data.

Although the formal errors indicate a significant difference between this period and that derived from the Loiano photometry alone, we believe the true error in the period is larger than the formal errors. In Figure 2, the model light curves for both periods are plotted over the observed photometry. Even when considering the TNG data, neither period is obviously preferred. In addition, light curves folded at both periods look qualitatively similar. We therefore consider a realistic estimate on the systematic error in the period to be 0.0064 h, the difference between the two photometric periods.

Additional observations will be needed to determine the photometric period more precisely. If the photometric period of 2.94 h is the orbital period of the system, then KIC J1924+4459 lies within the $2-3$ h CV period gap.

No deep eclipses are observed. Small dips which could be grazing eclipses are visible just after minimum light in the Loiano data. These have been indicated in Figure 2 with vertical tick marks. The location of the tick mark at T=24.175 h after BJD 2454714.5 was set by visual inspection; all other tick marks are spaced by integer multiples of the photometric period of 2.9358 h. Thse dips are consistent with the photometric period throughout both Loiano data sets, but are not seen in the McDonald data. A longer data set, such as that being obtained by the Kepler mission, therefore will be required to address this issue.

After removing this long-period variability, the residual light curves from all four nights of data also show significant amplitude ($\sim 5\%$) variability on time scales of $\sim 650s$ and $\sim 1200s$. Significant power is visible at these frequencies in the DFTs of the combined data (Fig. 3) and of each individual run. However, this variability is not fully coherent, even within a single observation, indicating that these are not non-radial pulsations on the surface of the WD primary.

2.2.2. *Long-Term Variability*

We have been able to identify KIC J1924+4459 in several archival catalogs, including both epochs of the Palomar Observatory Sky Survey (POSS), the Lick Northern Proper Motion study, and 2MASS. Historic photometric data culled from the the Naval Observatory Merged Astrometric Dataset (NOMAD) are presented in Table 1. We note that the USNO-A2 catalog does not resolve KIC J1924+4459 and a similarly-bright optical companion star; we therefore do not include those data in this summary. Visual inspection of both epochs of the POSS reveals significant proper motion of KIC J1924+4459 relative to the optical companion, so these two sources are likely unrelated.

Even allowing for uncertainty in the photographic plate magnitudes, residual contamination from the neighbor star, and the uncertain phase of the recent digital photometry, it appears that KIC J1924+4459 may have faded by $\sim 0.5-1$ magnitude between the second-epoch POSS observations of the early 1990s and the 2MASS/KIC observations of the late 1990s and mid-2000s. Such fading episodes are observed in NLs of the VY Scl subclass. Given the uncertainties, however, we cannot conclusively state whether KIC J1924+4459 entered a VY Scl-like low state in the mid- to late 1990s.

3. SPECTROSCOPIC ANALYSIS

3.1. *Spectroscopic Observations*

Spectroscopic observations of KIC J1924+4459 were obtained with the Blue Channel spectrograph on the MMT on UT 2008 September 24 and 25. On the first night, a single 300 s exposure revealed broad hydrogen absorption with narrow emission cores; this led us to an initial interpretation that this object could be a WD+M binary.

On the second night, significant additional spectroscopy was obtained when high winds precluded observations of the spectroscopic run's primary targets. Data were obtained with a 500 grooves per millimeter grating blazed at 5410Å and a $1''$-wide slit; no order blocking filter was used. Wavelength coverage extends from 3200Å to 6300Å. The resulting spectral resolution, measured from isolated night-sky emission lines, gives a Gaussian full-width at half maximum (FWHM) of 3.8Å.

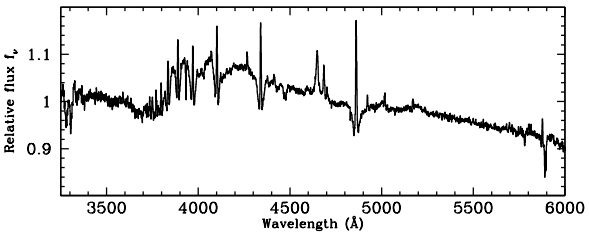

Figure 4. Averaged optical spectrum of KIC J1924+4459. The shallow, broad Balmer and He I absorption lines with emission cores, the strong He II and Bowen blend emission lines, and the appearance of the Balmer jump in emission are all typical of nova-like variables of the UX UMa class.

Nine 480-s exposures were obtained over 1.4 hours before winds forced dome closure, corresponding to nearly half of the suspected orbital period. In Figure 4, we show the average spectrum from these nine exposures. The spectrum is dominated by broad Balmer absorption with emission lines at the line core. He I λ4471 is also observed as a broad absorption line with an emission core. Numerous other weak He I lines are observed in emission only. Strong emission lines of He II λ4686 and the C III/N III Bowen blend emission near 4648Å are also present. Equivalent widths (EWs) of prominent absorption and emission lines are given in Table 2.

Strong, narrow Ca II K and Na I D lines are observed in absorption. As the source is located near the galactic plane ($b = +13\overset{\circ}{.}46$), these absorption features seem likely to be interstellar in origin. Using the dust maps of Schlegel et al. (1998), the estimated color excess due to dust extinction is $E(B-V) = 0.144$ mag, assuming all extinction is foreground to the system. Along the line of sight toward the CV, the total hydrogen column density is $1.21 \times 10^{21}\,\mathrm{cm}^{-2}$ (Dickey & Lockman 1990), implying an upper limit $E(B-V) \leq 0.18$. The EW of the Na D lines measured from our spectroscopy is 0.57 ± 0.02Å; based on the empirical relation of interstellar Na D strength to $E(B-V)$ of Munari & Zwitter (1997), our measurement implies a significantly higher $E(B-V) \approx 0.45 \pm 0.15$. This suggests that KIC J1924+4459 is either reddened substantially by patchy interstellar extinction, or that significant Na D absorption is intrinsic to the system.

3.2. *Radial velocity variations*

We searched for evidence of radial velocity variations by cross-correlating each individual spectrum with the first spectrum. Continuum, including the broad Balmer absorption, was fit and subtracted, so that the cross-correlation results in the emission line velocity curve. These relative velocities are listed in Table 3, and the resulting radial velocity curve is shown in Figure 5.

We detect small but significant radial velocity variations. Working under the assumption that these variations are intrinsic orbital motions, that the orbital

Table 2
Equivalent Widths of Prominent Lines in KIC J1924+4459

Obs. Midpt. (BJD− 2450000)	S/N	Hβ total (Å)	Hβ emiss. (Å)	Hγ total (Å)	Hγ emiss. (Å)	He I λ4471 total (Å)	He I λ4471 emiss. (Å)	He I λ5876 (Å)	He II λ4686 (Å)	N III / C III (Å)
4734.60556	93	1.49 ± 0.29	-2.48 ± 0.04	1.65 ± 0.10	-1.38 ± 0.02	0.31 ± 0.03	-0.17 ± 0.01	-0.45 ± 0.03	-1.08 ± 0.18	-1.23 ± 0.07
4734.61133	90	1.01 ± 0.27	-0.74 ± 0.09	1.41 ± 0.32	-1.31 ± 0.02	0.40 ± 0.05	-0.14 ± 0.01	-0.38 ± 0.03	-0.74 ± 0.09	-1.30 ± 0.10
4734.61713	95	1.59 ± 0.25	-1.92 ± 0.05	1.24 ± 0.22	-1.42 ± 0.01	0.25 ± 0.05	-0.11 ± 0.02	-0.38 ± 0.03	-0.42 ± 0.09	-1.40 ± 0.13
4734.62292	111	1.18 ± 0.21	-2.23 ± 0.05	1.12 ± 0.17	-1.30 ± 0.01	0.46 ± 0.07	-0.11 ± 0.02	-0.23 ± 0.06	-0.41 ± 0.09	-1.38 ± 0.10
4734.62877	104	1.31 ± 0.07	-1.84 ± 0.04	0.92 ± 0.13	-1.42 ± 0.03	0.75 ± 0.09	-0.07 ± 0.01	-0.36 ± 0.08	-0.50 ± 0.08	-1.18 ± 0.17
4734.63649	105	0.95 ± 0.16	-1.89 ± 0.09	1.15 ± 0.05	-1.27 ± 0.03	0.49 ± 0.09	-0.03 ± 0.02	-0.08 ± 0.15	-0.57 ± 0.09	-1.17 ± 0.07
4734.64229	101	1.46 ± 0.16	-1.86 ± 0.07	1.34 ± 0.20	-1.04 ± 0.04	0.56 ± 0.04	-0.02 ± 0.03	-0.07 ± 0.14	-0.45 ± 0.07	-1.01 ± 0.13
4734.64807	99	1.14 ± 0.27	-1.86 ± 0.04	1.47 ± 0.11	-1.02 ± 0.05	0.51 ± 0.05	0.00 ± 0.04	-0.02 ± 0.14	-0.23 ± 0.05	-1.30 ± 0.11
4734.65769	94	1.18 ± 0.27	-2.05 ± 0.09	1.45 ± 0.19	-1.25 ± 0.02	0.51 ± 0.09	-0.03 ± 0.02	-0.11 ± 0.14	-0.41 ± 0.04	-1.55 ± 0.12
Averaged	211	1.45 ± 0.10	-1.97 ± 0.03	1.26 ± 0.20	-1.19 ± 0.02	0.50 ± 0.05	-0.05 ± 0.03	-0.25 ± 0.09	-0.48 ± 0.04	-1.29 ± 0.04

Table 3
Emission line relative radial velocity measurements for KIC J1924+4459

Obs. Midpt. (BJD-2450000)	All Lines	Hβ	Hδ–H8	He II λ4686	N III/C III
4734.60556	...	...	...	...	...
4734.61133	-2.8 ± 10.3	1.0 ± 6.5	-4.4 ± 6.3	-19.4 ± 11.5	-61.9 ± 11.1
4734.61713	7.7 ± 9.4	14.0 ± 6.6	2.4 ± 6.5	-6.9 ± 7.0	-32.1 ± 11.4
4734.62292	19.8 ± 14.3	20.5 ± 4.7	30.1 ± 8.4	29.0 ± 14.5	-2.9 ± 12.1
4734.62877	23.0 ± 10.0	34.6 ± 5.9	21.6 ± 8.6	-13.1 ± 13.6	-16.4 ± 11.0
4734.63649	36.7 ± 14.3	51.5 ± 5.4	33.9 ± 10.1	9.0 ± 15.5	15.3 ± 7.4
4734.64229	18.7 ± 10.1	34.9 ± 5.6	22.2 ± 10.6	-39.8 ± 13.3	-20.5 ± 9.2
4734.64807	18.6 ± 12.7	35.2 ± 5.5	15.1 ± 7.4	-49.0 ± 15.6	-39.4 ± 11.4
4734.65769	6.6 ± 15.2	3.1 ± 4.4	6.4 ± 6.7	-6.8 ± 21.6	-18.8 ± 8.2

Note. — Velocities are in km s^{-1} and relative to first observation.

period is equal to the primary photometric period of $P_{\rm phot} = 2.9358$ h, and that the orbit is circular, we use least-squares fitting to determine an orbital solution of the form:

$$v_{r,rel} = \gamma + K \cos(2\pi \frac{t - t_{0,\rm spec}}{P}) \,. \qquad (2)$$

The resulting fit (shown in Figure 5) gives $K = 30.1 \pm 11.8$ km s^{-1}, $t_{0,\rm spec}$(BJD) = 2454734.63588(383), and $\gamma = -6.4 \pm 9.2$ km s^{-1}. The goodness-of-fit is very high, with $\chi^2/\nu = 0.4$. We note that the photometric period may not be the orbital period, but the photometric modulation could be due to some other phenomenon such as a superhump. To confirm whether the photometric period traces the true orbital motion or a superhump period, longer spectroscopic coverage is needed.

The absolute systemic radial velocity $\gamma_{\rm abs}$ is obtained by cross-correlating the continuum-subtracted emission line spectrum with a artificial zero-velocity Balmer emission spectrum; this velocity was corrected to the local standard of rest using the standard solar motion. This exercise gives $\gamma_{\rm abs} = -32.14 \pm 9.2 \pm 17.7$ km s^{-1}, where the first error is the error arising from the orbital solution and the second error is the uncertainty in the absolute heliocentric velocity determination.

Defining zero spectroscopic phase as the red-to-blue velocity crossing, the time of zero phase $T_{0,\rm spec}$(BJD) = 2454734.66646(383). Based on Equation 1 and including the accumulated systematic uncertainty in the photometric period determination, this corresponds to a photometric phase $(t-t_{0,\rm phot})/P = 0.47 \pm 0.30$. The relatively large accumulated uncertainty in photometric phase therefore precludes precise comparison of these spectroscopic data with the photometry at this time.

Many CVs show different γ and K values for different emission lines due to their different origins within the system. Therefore, we also calculated the radial velocity curves subsets of the emission lines, including Hβ, the higher-order Balmer lines (Hδ–H8), He II, and the Bowen blend line. The relative velocities for these subsets of lines are listed in Table 3 and plotted in Figure 5.

Radial velocity curves were determined by fitting these velocities with a sinusoid of a fixed period of 2.9358 h. From Hβ velocities alone, the resultant $K = 51.1 \pm 4.8$ km s^{-1}, significantly higher than the fit using all the lines, though the fit is significantly worse ($\chi^2/\nu = 4.4$). Within the errors, γ is unchanged. The fit to the higher-order Balmer lines are, within the errors, consistent with the initial fit obtained using all emission lines.

The individual sinusoidal fits to He II and the Bowen blend were significantly different than the initial and Balmer line fits. For He II, $K = 33.9 \pm 13.8$ km s^{-1} and $\gamma = -34.0 \pm 11.8$ km s^{-1} with $\chi^2/\nu = 4.3$. For the Bowen blend, $K = 15.2 \pm 9.1$ km s^{-1}, $\gamma = -24.4 \pm 6.6$ km s^{-1}, and $\chi^2/\nu = 9.0$. Within the errors, these amplitudes are consistent with one another, yet of lower amplitude than the Hβ variations, as would be expected since higher-excitation lines generally originate much closer to the accreting white dwarf. However, these fits are only slightly favored over the weighted means (constant velocity solutions) of -11.0 ± 3.6 km s^{-1} (He II, $\chi^2/\nu = 4.7$) and -17.8 ± 2.7 km s^{-1} (C III/N III, $\chi^2/\nu = 8.1$). As

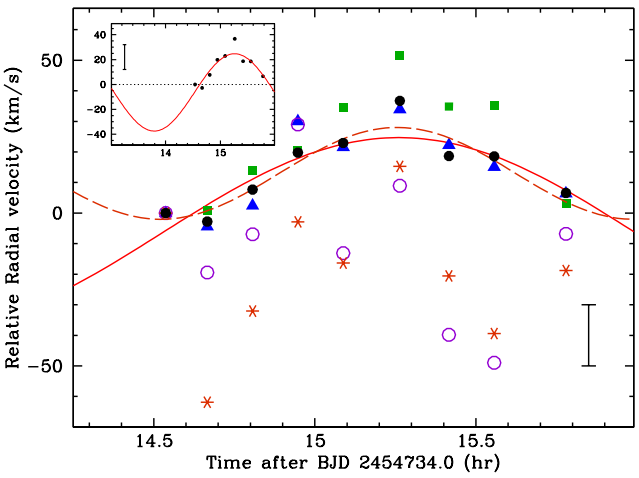

Figure 5. Radial velocity measurements for KIC J1924+4459 based on MMT low-resolution spectroscopy. Points indicate relative velocities for all emission lines (filled circles), Hβ emission lines only (filled squares), Balmer emission lines of Hδ through and including H8 (filled triangles), He II emission (open circles), and the C III/N III Bowen blend emission (asterisks). The error bar in the lower right shows a typical uncertainty ($\pm$10 km s^{-1}) in the relative velocity measurements; individual errors are given in Table 3. The solid curve is the best-fit sinusoid to all emission lines assuming the orbital period to be equal to the photometric period; the dashed curve is the best fit sinusoid to all data assuming an orbital period of half the photometric period. The inset shows one complete photometric cycle; our measurements span roughly half the photometric period. The Balmer emission line motion may be indicative of orbital motion.

the radial velocities of these high-excitation lines are observed to vary rapidly in some other CVs, particularly in some SW Sex systems, we again caution that additional observations are necessary and that these sinusoidal fits may not have any physical meaning.

3.3. *Emission Line Structure and Strength*

The emission lines, including the Balmer series lines, are resolved in the individual spectra (Table 4). For comparison purposes, the measured FWHM of the unresolved [O I] λ5577 night sky line is included in the table. Mean velocity widths (FWHM) of the Balmer lines are 330 ± 20 km s^{-1} after correcting for the instrumental resolution; He I lines are similarly narrow. The width of He II λ4686 may be somewhat broader; $\approx 375 \pm 15$ km s^{-1}. In the summed spectrum, no evidence for double-peaked emission lines is seen.

The emission line strengths of all emission lines, with the exception of the Bowen blend, are observed to vary significantly as a function of time (Table 2, Figure 6). In particular, the He I lines (λ4471 and λ5876) both vanish toward later times, and the He II λ4686 line is significantly stronger in the first two exposures than in later exposures; the Hβ emission line may show similar behavior. The Bowen blend emission has a mean EW of -1.29 ± 0.04 Å; all individual data points are within 2σ measurement errors of this mean value, so any intrinsic variability in the EW of this line must be $\lesssim 0.2$ Å in amplitude.

Figure 7 compares equivalent widths for pairs of emission lines in four cases where a significant correlation

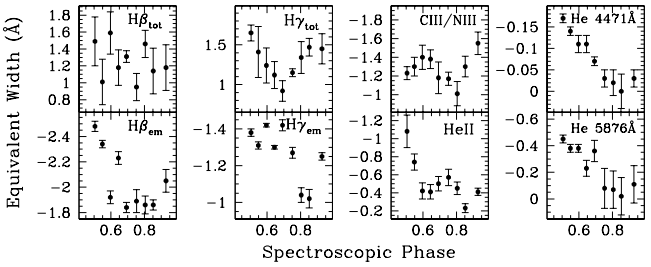

Figure 6. Equivalent widths of prominent spectral features as a function of spectroscopic phase; zero phase is defined as the red-to-blue velocity crossing. Vertical axes are oriented such that stronger measurements, whether of emission or absorption lines, are toward the top. Balmer and He I emission lines show obvious trends with phase; the He II emission line appears quite strong in the first two observations.

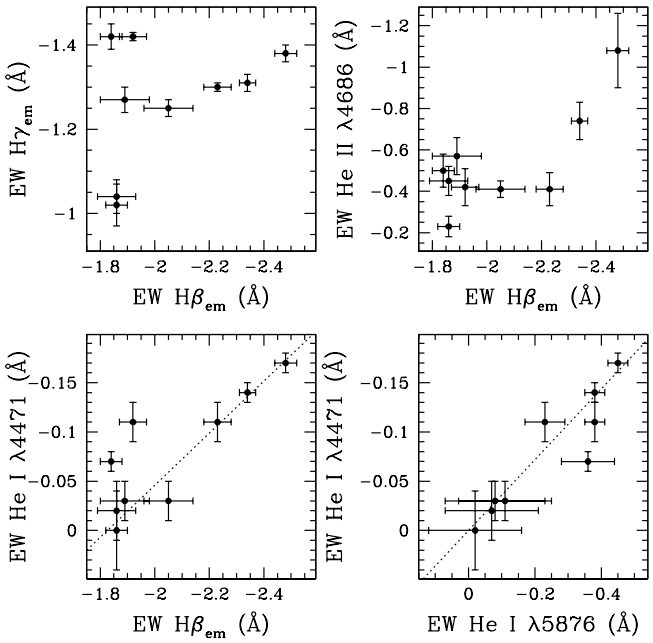

Figure 7. Comparison of equivalent widths of various emission lines. Dotted lines indicate linear correlations with slopes given in the text. While the correlation of Hβ with Hγ shows significant scatter when Hβ emission is weak, the other correlations are strong.

is observed. Hβ and Hγ emission is correlated, as would be expected, though there is significant scatter at weaker Hβ strengths. This could be indicative of different emission mechanisms being observed at different phases, or of systematic problems in measuring the emission line strengths in one or both lines. Hβ and He I λ4471 show a nearly linear correlation with EW(λ4471)/EW(Hβ) = 0.26. Likewise, the equivalent widths of He I λ4471 and He I λ5876 are linearly correlated; EW(λ4471)/EW(λ5876) $\approx$ 0.36. Finally, the two spectra with strongest He II emission also exhibit the strongest Hβ emission.

Lastly, the strong He II line might suggest that KIC J1924+4459 could be a source of X-ray emission. Searches of the available X-ray catalogs via the

Table 4
Emission line widths in KIC J1924+4459

Obs. Midpt. (BJD-2450000)	[O I] λ5577 (Å)	Hβ FWHM (Å)	Hβ σ km s^{-1}	Hγ FWHM (Å)	Hγ σ km s^{-1}	He II λ4686 FWHM (Å)	He II λ4686 σ km s^{-1}	N III/C III FWHM (Å)
4734.60556	3.85	7.59	172	6.22	144	9.75	244	15.45
4734.61133	3.82	6.93	152	5.80	129	8.87	218	14.11
4734.61713	3.82	6.78	147	7.28	182	6.41	140	17.77
4734.62292	3.77	7.54	171	6.21	144	5.93	123	14.74
4734.62877	3.79	6.71	145	6.72	163	7.24	168	13.33
4734.63649	3.77	6.74	146	6.85	167	8.09	194	12.16
4734.64229	3.75	7.45	168	6.31	148	6.63	148	11.14
4734.64807	3.75	7.06	156	5.58	120	6.24	134	13.22
4734.65796	3.75	6.53	139	5.78	128	6.87	156	20.61
Average	3.82	6.20	128	7.39	186	6.94	158	14.90

Note. — Velocity dispersions, but not FWHMs, are corrected for average instrumental broadening of FWHM= 3.82Å. The FWHM of the telluric [O I] auroral line is shown to illustrate the instrumental broadening and typical scatter in the measurements. No velocity dispersion is calculated for the N III/C III Bowen blend.

HEASARC archive fail to result in any coincident X-ray sources within 10′ of the star.

4. CLASSIFICATION AND IMPLICATIONS

4.1. *A nova-like variable of the UX UMa class*

To summarize our observations, we find that the star KIC J1924+4459 is a photometric variable with a period of ≈ 2.94 h and shows spectral characteristics of CVs; hence it is a cataclysmic variable in the 2−3 h period gap. Time-series photometry shows no deep eclipses. Quasi-periodic variations are also observed on time scales of ≈ 1200 s and ≈ 650 s. The spectrum exhibits Balmer absorption with resolved, single-peaked emission line cores, as well as strong He II and Bowen blend emission. Radial velocity variations are observed that are consistent with low-amplitude motion and have periods either close to the photometric period or close to half of the photometric period. However, the phase coverage is currently too small to study the spectral and radial velocity variability in detail.

KIC J1924+4459 is clearly a NL variable of the UX UMa class. The strong, persistent Balmer absorption features indicate that this is a system accreting at a high rate. The strength of UX Uma emission features varies from object to object (Dhillon 1996). Quasi-periodic short-term photometric variability is also a common feature observed in most NLs. KIC J1924+4459 is consistent with all of these descriptors. We roughly estimate the accretion rate via two methods. First, the small EW of Hβ emission implies a limit on the disk luminosity of $M_V \leq 6$, or a lower limit on the accretion rate of $\dot{M} \gtrsim 3 \times 10^{-10}\, M_\odot\, \mathrm{yr}^{-1}$ (Patterson 1984). Based on magnetic braking calculation by McDermott & Taam (1989), the secular accretion rate for a orbital period of 2.94 h is $\dot{M} = 1.1 \times 10^{-9}\, M_\odot\, \mathrm{yr}^{-1}$. This should be considered a lower limit, as most CVs with periods $\sim 3-4$ h have higher secular accretion rates of $\dot{M} \gtrsim 2 \times 10^{-9}\, M_\odot\, \mathrm{yr}^{-1}$ (e.g., Howell et al. 2001; Townsley & Bildsten 2003).

Archival photographic plate photometry suggests that this star may have been up to a magnitude brighter in the past than when imaged as part of the Kepler Input Catalog survey, hinting that this star may have been (or even still be) in a VY Scl-type low state. However, the data are sparse, and the historical magnitudes could be in error due to the close optical companion star.

We calculate a lower limit on the distance to KIC J1924+4459 using the archival 2MASS photometry, under the assumption that the J-band detection is due totally to the secondary (donor) star. Knigge (2006) calculates that the donor would be of spectral type M4.2 with $M_J = 7.88$ at the edge of the period gap. Accounting for the Galactic extinction from Schlegel et al. (1998), the intrinsic distance modulus is $(m - M)_0 = 8.83 \pm 0.14$, or 583^{+39}_{-36} pc. If, instead, we adopt the reddening of $E(B-V) = 0.45 \pm 0.15$ derived from the Na D EW measurements, the intrinsic distance modulus is 8.55 ± 0.19, or 513^{+47}_{-43} pc.

4.2. *Potential SW Sex characteristics*

The photometric properties of KIC J1924+4459 are consistent with, though not exclusive to, NLs of the SW Sex class. The photometric period is within the CV period gap, and the light curve does not show deep eclipses. SW Sex systems account for 55% of CVs in the period gap (Rodríguez-Gil et al. 2007a), and 37% of SW Sex systems do not show eclipses (Rodríguez-Gil et al. 2007b). The time scale and amplitude of the quasi-coherent variability is similar to that observed in a number of NLs of the SW Sex class (Rodríguez-Gil et al. 2007b,a).

One defining spectral characteristic of SW Sex stars are single-peaked Balmer and He I emission lines (Warner 1995), such as we observe in KIC J1924+4459. Additional defining spectral characteristics of the SW Sex stars include a higher-velocity emission S-wave and variable absorption components in the trailed spectrum. We are, unfortunately, unable to identify these features in our data due to the combination of the low velocity amplitude, the low resolution of these spectra, and the small phase coverage of these data. A longer set of time-series data at higher spectral resolution are needed to search for this diagnostic signature. Likewise, the phase delay in the red-to-blue crossing of the Balmer lines that is characteristic of many SW Sex systems cannot be tested with these data due to the inability to determine the absolute phase of the system in this short run of data.

In summary, we speculate that KIC J1924+4459 is a member of the rapidly-growing SW Sex class of CV based

on our data, which are consistent with common definitions of SW Sex stars. However, the data are not sufficient to make a definitive identification at this time.

4.3. *Implications and future potential*

The discovery of a new CV, and in particular a potential SW Sex type system, in the $2-3$ h period gap is not only important to increase the statistics of this emerging class of accreting CVs, but also to help understand the crucial role of angular momentum loss mechanisms that act at these periods (for details, see Townsley & Gänsicke 2009, and references therein). Systems in the period gap are believed to be transition systems. Angular momentum loss is believed to be driven by magnetic breaking for CVs above the gap and driven by gravitational radiation in and below the gap. The fact that many CVs in the gap, at least half of which are SW Sex objects, display features indicating high $\dot{M}$ when this is not expected by angular momentum loss theory is a problem that needs to be solved. Therefore, the study of these systems is crucial to a better understanding of CV evolution.

This system requires further careful observations in order to classify the CV securely. In particular, confirming whether KIC J1924+4459 is a SW Sex-class system will require time-resolved, high resolution spectroscopy. (Spectro-)polarimetric and X-ray observations can provide evidence of the presence or absence of strong magnetic fields on the accreting white dwarf. Long-term photometric monitoring and a more careful analysis of archival imaging may be able to determine if this system enters occasional VY Scl-like low states.

The identification of a cataclysmic variable in the field of view of the Kepler Mission provides the unprecedented opportunity to obtain long-term, uninterrupted photometric monitoring of such a system. First and foremost, coordinated observations combining Kepler data with ground-based spectroscopy and/or polarimetry could help in furthering our understanding of this system. Additionally, Kepler's superb photometric precision and long mission lifetime can provide a unique opportunity to search for very low-amplitude and low-frequency phenomena, and to open new avenues of data analysis for both this object and cataclysmic variable stars in general. Indeed, KIC J1924+4459 is targeted for short-cadence observations by the Kepler Asteroseismic Science Consortium (KASC) during roll 3 of the Kepler mission; these data will soon be available.

KAW is grateful for the financial support of National Science Foundation award AST-0602288. DDM acknowledges the financial support of INAF PRIN-INAF-17/07. The authors wish to thank Arnold Klemola, Bob Hanson, Dave Monet, and Tim Brown for their great assistance in tracking down dates of observations for the archival photometric data. RS wishes to thank Alfio Bonanno and Silvio Leccia, who agreed to devote part of their TNG run to the *Kepler pulsator candidates* program following technical problems with the SARG instrument, and the TNG technical team, Gloria Andreuzzi, Antonio Magazzu and Luca Di Fabrizio, for the excellent job during the service-mode observations. Ed Sion, Paula Szkody, Steve Howell, and James Liebert all provided insightful discussions and advice in interpreting these results. We are also grateful to Mukremin Kilic and Susan Thompson for taking additional spectroscopic and photometric data that were, alas, not used in this analysis. Fergal Mullally kindly provided assistance in calculating barycentric corrections for the spectroscopy. The authors thank the anonymous referee for their time and useful comments regarding this paper.

REFERENCES

Baskill, D. S., Wheatley, P. J., & Osborne, J. P. 2005, MNRAS, 357, 626
Casares, J., Martinez-Pais, I. G., Marsh, T. R., Charles, P. A., & Lazaro, C. 1996, MNRAS, 278, 219
Dhillon, V. S. 1996, in Astrophysics and Space Science Library, Vol. 208, IAU Colloq. 158: Cataclysmic Variables and Related Objects, ed. A. Evans & J. H. Wood, 3–+
Dickey, J. M., & Lockman, F. J. 1990, ARA&A, 28, 215
Hoard, D. W., Szkody, P., Froning, C. S., Long, K. S., & Knigge, C. 2003, AJ, 126, 2473
Howell, S. B., Nelson, L. A., & Rappaport, S. 2001, ApJ, 550, 897
Knigge. C. 2006, MNRAS, 373, 484
Latham, D. W. 2008, Physica Scripta Volume T, 130, 014034
McDermott, P. N. & Taam, R. E. 1989, ApJ, 342, 1019
Mullally, F., Thompson, S. E., Castanheira, B. G., Winget, D. E., Kepler, S. O., Eisenstein, D. J., Kleinman, S. J., & Nitta, A. 2005, ApJ, 625, 966
Mullally, F., Winget, D. E., Degennaro, S., Jeffery, E., Thompson, S. E., Chandler, D., & Kepler, S. O. 2008, ApJ, 676, 573
Munari, U., & Zwitter, T. 1997, A&A, 318, 269
Nather, R. E., & Mukadam, A. S. 2004, ApJ, 605, 846
O'Donoghue, D., Kanaan, A., Kleinman, S. J., Krzesinski, J., & Pritchet, C. 2000, Baltic Astronomy, 9, 375
Patterson, J. 1984, ApJS, 54, 443
Rodríguez-Gil, P., & Martínez-Pais, I. G. 2002, MNRAS, 337, 209
Rodríguez-Gil, P., Casares, J., Martínez-Pais, I. G., Hakala, P., & Steeghs, D. 2001, ApJ, 548, L49
Rodríguez-Gil, P., Casares, J., Martínez-Pais, I. G., & Hakala, P. J. 2002, The Physics of Cataclysmic Variables and Related Objects, 261, 533
Rodríguez-Gil, P., et al. 2007a, MNRAS, 377, 1747
Rodríguez-Gil, P., Schmidtobreick, L., & Gänsicke, B. T. 2007b, MNRAS, 374, 1359
Rodríguez-Gil, P., Martínez-Pais, I. G., & de La Cruz Rodríguez, J. 2009, MNRAS, 395, 973
Schlegel, D. J., Finkbeiner, D. P., & Davis, M. 1998, ApJ, 500, 525
Silvotti, R., Handler, G., Schuh, S., Castanheira, B., & Kjeldsen, H. 2009, Communications in Asteroseismology, 159, 97
Smith, D. A., Dhillon, V. S., & Marsh, T. R. 1998, MNRAS, 296, 465
Thorstensen, J. R. 1986, AJ, 91, 940
Thorstensen, J. R., Ringwald, F. A., Wade, R. A., Schmidt, G. D., & Norsworthy, J. E. 1991, AJ, 102, 272
Townsley, D. M., & Bildsten, L. 2003, ApJ, 596, L227
Townsley, D. M., & Gänsicke, B. T. 2009, ApJ, 693, 1007
Warner, B. 1995, Cataclysmic Variable Stars (Cambridge University Press)
Williams, R. E. 1989, AJ, 97, 1752